Scientia Iranica B (2014) 21(1), 119–129

SCIENTIA IRANICA

Sharif University of Technology
Scientia Iranica
Transactions B: Mechanical Engineering
www.scientiairanica.com

Numerical simulation of oblique impact of a droplet on a surface in the film boiling regime

P. Pournaderi and A.R. Pishevar*

Department of Mechanical Engineering, Isfahan University of Technology, Isfahan 84156-83111, Iran.

Received 26 November 2011; received in revised form 12 March 2013; accepted 9 September 2013

KEYWORDS
Oblique impact;
Leidenfrost regime;
Droplet;
Hot surface;
Level set;
Ghost fluid method.

Abstract. In this study, we focused on simulation of the oblique collision of a water droplet on a superheated surface via a novel algorithm. In this approach, the vaporization rate of the droplet is computed and is accurately applied in the solution process. The high temperature of the surface leads to the formation of a vapor layer between the droplet and surface. Mesh clustering near the surface is used to capture the effect of the vapor layer. The level set method, in conjunction with the ghost fluid method, is used to represent a sharp interface. Available experiments confirmed the validity of the proposed algorithm. The Weber number based on normal velocity is the dominant parameter in the oblique impact process. The spreading radius and contact time of the droplet are dependent on the normal Weber number. An increase in the initial normal velocity of the droplet enhances the total heat removal from the wall.

1. Introduction

Depending on surface temperature, different regimes are expected when a droplet impacts on a surface. Above a certain temperature, called Leidenfrost temperature, the droplet does not wet the surface. This is due to the formation of a vapor layer between the droplet and surface. Vapor has low conductivity in comparison with liquid. Therefore, formation of a vapor layer reduces the heat flux dissipated from the wall and, consequently, increases the life time of the droplet. This regime is known as film boiling or the Leidenfrost regime.

Impingement of droplets on superheated surfaces is observed in many industrial applications. Specifically, we can refer to the steel industry. One of the important processes in the steel industry is the quenching or fast cooling of a part. The cooling method has a significant effect on the strength of the final product. When the heat transfer rate is very high, a more uniform quenching is obtained and, as a result, parts with better mechanical properties are produced. There is a similar situation in the casting process. Spray cooling has advantages that make it a suitable option for the quenching process. These advantages are high heat transfer rate, uniformity of temperature distribution in the part and lower dissipation of coolant material. Many researchers have studied droplet impingement on superheated walls experimentally. Wachters and Westerling [1] investigated the normal impact of saturated water droplets on a superheated wall. In this study, the Weber number, and the ratio of inertial force to surface tension force, was introduced as the dominant parameter in the Leidenfrost regime. Based on the Weber number, three different regimes were observed in their experiments. When the Weber number is less than 30, after spreading and recoiling stages, the droplet rebounds from the wall. In this case, surface tension force is dominant and

*. *Corresponding author. Tel.: +98 311 3915208; Fax: +98 311 3912628; Mobile: +98 9133130326*
E-mail addresses: s.pournaderi@me.iut.ac.ir (P. Pournaderi); apishe@cc.iut.ac.ir (A.R. Pishevar)

no secondary droplet is produced in the rebounding stage. When the Weber number is increased to a value greater than 30 but less than 80, the spreading and recoiling stages are the same as in the previous case. But, at the rebounding stage, one or two secondary droplets can be produced. For Weber numbers greater than 80, due to domination of the inertia force during the initial stage of the impact process, splashing occurs and a number of small droplets are produced. Hatta et al. [2] studied the impact of water droplets on different superheated metallic surfaces. They used droplets with different sizes and impact velocities. Karl and Frohn [3] reported different regimes in the oblique impact process. The observed regimes were similar to normal impingement cases. They found that when the impact energy is very low (We $\ll 1$), the droplet rebound is almost elastic. This regime is called the perfect reflection regime. With more increase in Weber number, the normal velocity after impact reduces considerably in comparison to its value before impact. For this case, the Weber number is still below 30. This regime is called the regular reflection regime. For Weber number greater than 30, depending on the value of the Weber number, secondary droplet formation or splashing occurs. The influence of the surface temperature and impingement angle on the impact process was investigated by Kang and Lee [4]. For surfaces with temperatures less than Leidenfrost temperature, no droplet rebound was observed. They also concluded that in the film boiling regime, the normal momentum of the droplet has the most effect on the dynamic behavior of the droplet after impingement. Biance et al. [5] investigated the elasticity of saturated droplets impacting on a superheated wall. They observed a quasi elastic rebound regime for very low Weber number (We $\ll 1$). The elasticity of the droplet decreases with increase in Weber number. Chen et al. [6] studied the impact of diesel oil droplets on horizontal and inclined surfaces. They found that for diesel droplets, the disintegration Weber number is not the same as that reported for other liquids.

There are also some numerical studies about droplet impingement on superheated surfaces. Deformation of micron subcooled droplets during impingement on a heated surface was studied by Karl et al. [7], numerically and experimentally. The volume of fluid method was employed for interface capturing in their numerical simulation. They satisfied the non-wetting condition by imposing a 180° contact angle and free slip condition for velocity. Harvie and Fletcher [8] modeled the vapor layer by solving axisymmetric equations of motion and neglecting convective terms. They also solved temperature equations in solid, liquid and vapor phases. In their proposed model, droplet vaporization was neglected and the effect of the vapor layer pressure was included as a source term in momentum equations. Using the vapor layer model, in conjunction with the volume of fluid method, they could only simulate impacts with low energies (We < 30) [9]. Ge and Fan [10] improved the vapor layer model of Harvie and Fletcher by adding convection terms in vapor layer calculations. Using a smeared out formulation of the level set method, they could simulate saturated impacts with low and moderate Weber numbers (We < 80). Chatzikyriakou et al. [11] applied a smeared out formulation of the level set method for simulation of saturated droplet impingement on a hot wall in the film boiling regime. Based on available experiments, a constant vaporization rate was employed for all surfaces of the droplet. With great simplification, this constant vaporization rate was only considered in the level set equation. In previous work, researchers mainly studied the normal impact of droplets on hot surfaces. Since, in practical cases, we encounter oblique collision of droplets on hot surfaces, this research focuses on oblique impact in the regular reflection regime. In spite of previous studies, the vaporization rate is computed and is accurately applied in the solution process. The level set method, in conjunction with the ghost fluid method, is used to model the interface in a sharp fashion. Mesh is clustered near the wall to capture the effect of the vapor layer accurately. Our code is verified against available experimental results. The effect of the initial normal velocity of the droplet on the cooling performance of the impact process is considered.

2. Basic equation

2.1. Flow and heat equations

All phases are supposed to be incompressible. Therefore, the mass and momentum conservation equations can be written as:

$$\nabla.\vec{V} = 0, \tag{1}$$

$$\frac{\partial \vec{V}}{\partial t} + (\vec{V}.\nabla)\vec{V} + \frac{\nabla p}{\rho} = \frac{(\nabla.\tau)^t}{\rho} + \vec{g}, \tag{2}$$

where $\vec{V} = (u, v, w)$ is the velocity vector, p is the pressure, ρ is the density, $\vec{g}$ is the gravity vector, T is the transpose operator and τ is the viscous stress tensor, defined as:

$$\tau = \mu \begin{pmatrix} \nabla u \\ \nabla v \\ \nabla w \end{pmatrix} + \mu \begin{pmatrix} \nabla u \\ \nabla v \\ \nabla w \end{pmatrix}^t. \tag{3}$$

μ is the dynamic viscosity. The following energy equation is used for calculation of the temperature field:

$$\frac{\partial T}{\partial t} + (\vec{V}.\nabla)T = \frac{\nabla.(k\nabla T)}{\rho C_p}. \tag{4}$$

In the above equations, T is the temperature, k is

the thermal conductivity and C_p is the specific heat at constant pressure.

2.2. Jump conditions

Fedkiw et al. [12] introduced the ghost fluid method to model a contact discontinuity in Euler equations. This method was extended by Liu et al. [13] for solving a variable coefficient Poisson equation with a specific jump condition at the interface. Later, this technique was employed for simulation of incompressible two phase flows [14-16]. In this approach, appropriate jump conditions are imposed at the interface accurately without smearing out variables across the interface. The main idea of this method is the use of ghost values in another phase for a discontinuous variable when crossing the interface. In this work, using the ghost fluid method, the interface is modeled in a sharp fashion.

The jump in quantity, A, across the interface, Γ, is defined as:

$$[A]_\Gamma = A_{g-}A_1, \tag{5}$$

where A_g and A_1 are the values of A in gas and liquid phases, respectively. Mass conservation across the interface in flows with phase change results in [14,15]:

$$\dot{m} = \rho_1(\vec{V}_{\text{int}} - \vec{V}_1).\vec{N} = \rho_g(\vec{V}_{\text{int}} - \vec{V}_g).\vec{N}. \tag{6}$$

$\dot{m}$ is the vaporization rate per unit surface and $\vec{N}$ is the unit normal vector to the interface. The interface velocity, $\vec{V}_{\text{int}}$, is defined as:

$$\vec{V}_{\text{int}} = \vec{V}_1 + \vec{V}_s. \tag{7}$$

$\vec{V}_s$ is the interface velocity due to vaporization, and can be obtained from a combination of Eqs. (6) and (7):

$$\vec{V}_s = \frac{\dot{m}}{\rho_1}\vec{N}. \tag{8}$$

Also, using Eqs. (6) and (7), the velocity jump condition can be derived as:

$$[\vec{V}]_\Gamma = \dot{m}\left[\frac{1}{\rho}\right]_\Gamma \vec{N}. \tag{9}$$

Momentum conservation across the interface is used for pressure jump calculation:

$$[p]_\Gamma - 2[\mu]_\Gamma(\nabla u.\vec{N}, \nabla v.\vec{N}, \nabla w.\vec{N}).\vec{N} = \sigma\kappa - \dot{m}^2\left[\frac{1}{\rho}\right]_\Gamma. \tag{10}$$

σ is the surface tension and κ is the curvature at the interface.

Similarly, the temperature jump condition is obtained based on energy conservation across the interface:

$$h_{lg}\dot{m} + [k\nabla T.\vec{N}]_\Gamma = 0. \tag{11}$$

h_{lg} is the latent heat of vaporization. Since the droplet is at saturation state, Eq. (11) can be written as:

$$\dot{m} = \frac{-k_g \nabla T.\vec{N}\,|_g^\Gamma}{h_{lg}}. \tag{12}$$

The above equation is used for calculation of the vaporization rate.

Suppose that velocity components and their tangential derivatives are continuous across the interface. Using this assumption and applying momentum conservation across the interface, the following jump condition can be obtained [16]:

$$\begin{pmatrix} [\mu u_x] & [\mu u_y] & [\mu u_z] \\ [\mu v_x] & [\mu v_y] & [\mu v_z] \\ [\mu w_x] & [\mu w_y] & [\mu w_z] \end{pmatrix} = [\mu] \begin{pmatrix} \nabla u \\ \nabla v \\ \nabla w \end{pmatrix} \begin{pmatrix} \vec{O} \\ \vec{T}_1 \\ \vec{T}_2 \end{pmatrix}^T \begin{pmatrix} \vec{O} \\ \vec{T}_1 \\ \vec{T}_2 \end{pmatrix} + [\mu]\vec{N}^T\vec{N} \begin{pmatrix} \nabla u \\ \nabla v \\ \nabla w \end{pmatrix} \vec{N}^T\vec{N} - [\mu] \begin{pmatrix} \vec{O} \\ \vec{T}_1 \\ \vec{T}_2 \end{pmatrix}^T \begin{pmatrix} \vec{O} \\ \vec{T}_1 \\ \vec{T}_2 \end{pmatrix} \begin{pmatrix} \nabla u \\ \nabla v \\ \nabla w \end{pmatrix} \vec{N}^T\vec{N}. \tag{13}$$

$\vec{T}_1$ and $\vec{T}_2$ are orthogonal unit tangent vectors at the interface. Viscous terms are calculated in a sharp fashion using the above equation. Due to the discontinuity of the velocity field in vaporizing flows, Eq. (13) is not valid for this kind of flow. Tanguy et al. [17] presented a solution for this problem, which is described in Section 3.1.

2.3. Level set method

In this research, the interface is captured by the level set method [18,19]. In this approach, the interface is assumed as the zero level set of a scalar function, φ. The level set function is defined as a signed distance function from the interface. This function is advected via the following equation:

$$\frac{\partial\varphi}{\partial t} + \vec{V}_{\text{int}}.\nabla\varphi = 0, \tag{14}$$

where $\vec{V}_{\text{int}}$ is given by Eq. (7). It is necessary to keep the level set function as a distance function during computations. Therefore, level set values obtained from Eq. (14) must be corrected via a reinitialization equation [20]:

$$\frac{\partial\varphi}{\partial\tau} = S(\varphi_0)(1- \mid \nabla\varphi \mid), \tag{15}$$

where τ is an artificial time, φ_0 is the value of φ before reinitialization and S is a smeared out sign function:

$$S(\varphi_0) = \frac{\varphi_0}{\sqrt{\varphi_0^2 + \varepsilon^2}}, \tag{16}$$

and $\varepsilon = \max(\Delta x, \Delta y, \Delta z)$. Often convergence to a steady state solution is achieved only by a few iterations.

One of the drawbacks of the level set method is losing the mass during computations. Son and Dhir [21] proposed the following equation to enforce mass conservation explicitly:

$$\frac{\partial \varphi}{\partial \tau} = (V_d - V_{d-r}) \mid \nabla \varphi \mid). \tag{17}$$

V_d is the droplet volume calculated from φ and V_{d-r} is the real volume of the droplet that satisfies mass conservation which is computed as:

$$V_{d-r} = V_{d0} - \frac{1}{\rho_1} \int_0^t \int_A \dot{m}\, dA\, dt, \tag{18}$$

where V_{d0} is the initial droplet volume and A is the instantaneous droplet surface. Having the level set function, unit normal vector $\vec{N}$ and curvature κ can be computed as:

$$\vec{N} = \frac{\nabla \varphi}{\mid \nabla \varphi \mid}, \tag{19}$$

$$\kappa = -\nabla . \vec{N}. \tag{20}$$

3. Numerical procedures

Governing equations are discretized on a staggered grid using the finite difference method. A standard projection method is used to solve flow equations. In all equations, a fifth order WENO method is used for discretization of convection terms. Diffusion terms are discretized by the standard central approximation. A third order TVD Runge-Kutta method is used to advance the solution forward in time.

Accurate capturing of the vapor layer effect plays a significant role in our numerical procedure. Therefore, mesh is clustered near the wall to have an appropriate resolution of mesh in the vapor layer.

3.1. Solving flow equations

Flow equations are solved using a standard projection method. The ghost fluid method is applied for sharp calculation of discontinuous variables via imposing appropriate jump conditions. As previously mentioned, due to the discontinuity of the velocity field, Eq. (13) is not valid for vaporizing flows. We applied the procedure proposed by Tanguy et al. [17] for solving this problem. The velocity jump condition is used to extend the velocity field of each phase into another phase:

$$\vec{V}_l^{\text{ghost}} = \vec{V}_g - \dot{m} \left[\frac{1}{\rho}\right]_\Gamma \vec{N}. \tag{21}$$

$$\vec{V}_g^{\text{ghost}} = \vec{V}_1 - \dot{m} \left[\frac{1}{\rho}\right]_\Gamma \vec{N}. \tag{22}$$

Therefore, we have two extended velocity fields which are continuous across the interface. Now, in the first step of the projection method, pseudo velocities are computed for liquid and gas extended fields separately. Eq. (13) is applied for each continuous velocity field. In the second and third steps of the projection method, new pressure and velocity fields are calculated. But, note that in each phase, the pseudo velocity related to that phase must be used.

3.2. Solving heat transfer equation

The heat transfer equation is discretized in time as follows:

$$T^{n+1} - \frac{\Delta t}{\rho C_p} \nabla . (k \nabla T^{n+1}) = T^n - \Delta t (\vec{V} . \nabla) T^n. \tag{23}$$

The above equation is very similar to a variable coefficient Poisson equation. Therefore, the procedure introduced by Liu et al. [13] can be used for the discretization of diffusion terms.

Eq. (11) implies that in vaporizing flows, heat flux and, as a result, temperature gradient, is discontinuous across the interface. Therefore, ghost values for the temperature in the other phase are needed for computation of convection terms. Linear extrapolation normal to the interface can be used for calculation of ghost values. An accurate linear extrapolation method was proposed by Aslam [22], which is based on solving partial differential equations. This approach contains two steps as follows:

$$\frac{\partial T_n}{\partial \tau} \pm (\vec{N} . \nabla) T_n = 0, \tag{24}$$

$$\frac{\partial T_n}{\partial \tau} \pm (\vec{N} . \nabla) T = T_n, \tag{25}$$

where:

$$T_n = (\vec{N} . \nabla) T, \tag{26}$$

and τ is an artificial time. Due to the constant temperature of the liquid phase, it is only necessary to extend the temperature field of the gas phase into the liquid phase by solving equations with a negative sign until steady state. An explicit first order upwind scheme is used for solving the above equations.

3.3. Vaporization rate calculation

Vaporization rate calculation is an important part of our computations. Therefore, it is necessary to estimate this parameter as accurately as possible. The vaporization rate must be calculated in a band around the interface. This is due to the use of a WENO scheme for discretization of velocity convection terms. The calculated vaporization rate must have no gradient in the direction normal to the interface. Thus, we propose the following procedure for accurate computation of the vaporization rate:

1. Use Eqs. (23) and (24) for linear extrapolation of the gas temperature field into the liquid phase.
2. Use Eq. (12) to calculate the vaporization rate for nodes inside the gas phase and adjacent to the interface.
3. Use the following equation for constant extrapolation of vaporization rate values from the gas phase into the liquid phase, in the direction normal to the interface:

$$\frac{\partial \dot{m}}{\partial \tau} - (\vec{N}.\nabla)\dot{m} = 0. \quad (27)$$

4. Use the following equation for constant extrapolation of vaporization rate values from the liquid phase into the gas phase, in the direction normal to the interface:

$$\frac{\partial \dot{m}}{\partial \tau} - (\vec{N}.\nabla)\dot{m} = 0. \quad (28)$$

4. Results and discussions

In this section, three dimensional results for both normal and oblique impacts are presented. The schematic of the problem in the $x - y$ plane can be observed in Figure 1. On all boundaries except the wall, free boundary conditions are applied. No slip condition is used for velocity on the solid boundary. The Dirichlet condition is applied for temperature on all boundaries ($T_{\text{boundary}} = 673.15$ K.). Water droplets are at saturation state ($T_{\text{sat}} = 373.15$ K.) and the initial gas temperature is 673.15 K. Based on the grid study results, in all simulations, resolution of mesh is 15 CPR (Cell Per Radius). However, mesh clustering is used near the wall so that the ratio of the smallest cell height to the droplet radius is about 0.03 in this region. In all simulations, time is measured from the moment of initial contact.

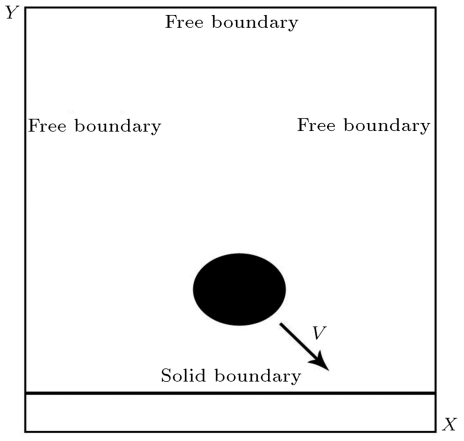

Figure 1. Schematic of the problem in $x - y$ plane.

4.1. Normal impact

In this section, the Wachters and Westerling experiment is used to verify the code and numerical procedure in which the impingement of a saturated water droplet, with a diameter of 2.3 mm and an initial velocity of 0.63 m/s on a surface with a temperature of 400°C, is considered. The Weber number ($\text{We} = \rho_1 V^2 D/\sigma$) for this case is 15; D and V are the droplet diameter and the droplet initial velocity, respectively.

Figure 2 represents the grid study results. Three different meshes are employed to ensure that the results are independent of the mesh size. A satisfactory convergence of the solution is observed. According to the results, a mesh with a resolution of 15 CPR is selected for simulations. Figure 3 shows the effect of mesh resolution on the droplet evaporation percent. In the film boiling regime, the droplet does not wet the surface, and the vapor layer acts as an insulator and reduces the heat transfer rate. On the other hand, the droplet contact time on the surface is very small. Therefore, only a small portion of the droplet is vaporized during the impact process. The results presented in Figure 3 confirm the convergence of the solution for mesh resolution greater than 15 CPR. Droplet deformation during the impact process can be seen in Figure 4. Due to initial kinetic energy, the droplet spreads and a liquid film forms on the surface. The resistance of surface tension and viscous forces slow the spreading process and, finally, the droplet

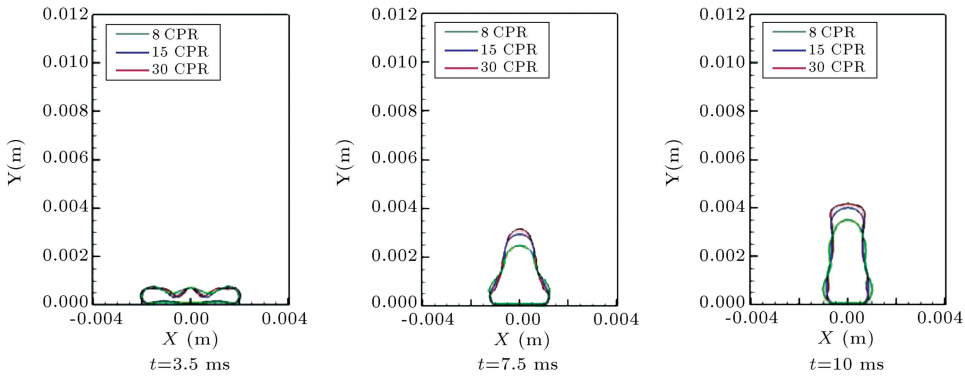

Figure 2. The effect of the mesh resolution on the droplet shape (We = 15, $D = 2.3$ mm and $T_w = 400$°C).

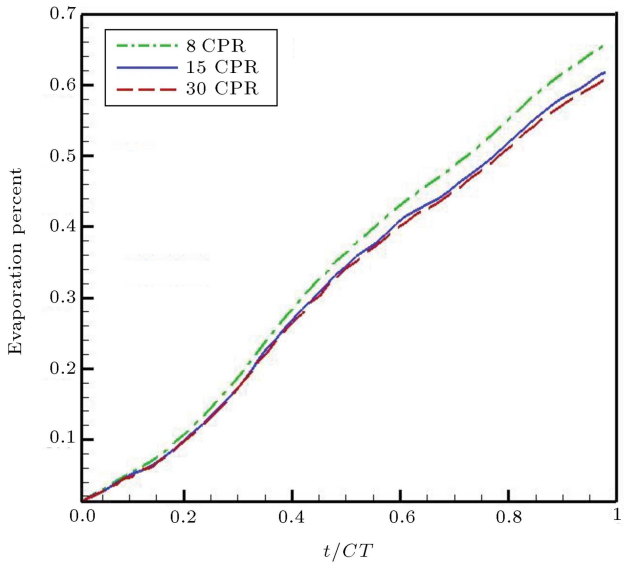

Figure 3. The effect of the mesh resolution on the droplet evaporation percent (We = 15, D = 2.3 mm and $T_w = 400°C$).

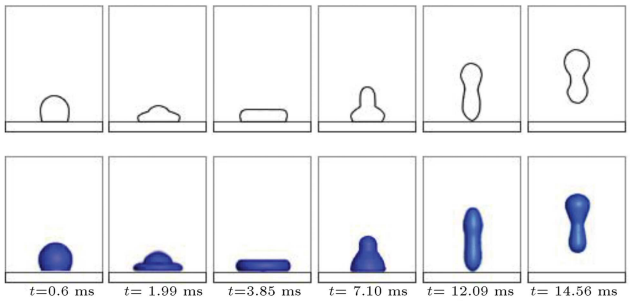

Figure 4. Droplet deformation during a normal impact process (We = 15, D = 2.3 mm and $T_w = 400°C$). Top and below figures represents experiment [1] and simulation results, respectively.

reaches its maximum spreading radius (t = 3.85 ms). In this moment, due to the high curvature of the liquid surface at the leading edge, the effect of surface tension becomes dominant and the droplet begins to recoil. After the droplet retracts sufficiently, an upward flow forms and the droplet bounces from the surface. In the film boiling regime, due to formation of the vapor layer, the droplet is not in direct contact with the surface. So, the effect of the wall friction is less and the droplet preserves most of its initial kinetic energy. This preserved energy causes the droplet to be able to bounce from the surface. As observed, there is a good agreement between simulation and experimental results, and the simulation can reproduce the shape of the droplet during the impact process.

4.2. Oblique impact

Now, the three dimensional results of oblique impact, which is the issue of interest in this research, are presented.

Similar to the previous simulation, consider that a saturated water droplet with a diameter of 2.3 mm impacts on a surface with a temperature of 400°C. However, in this case, in addition to an initial normal velocity, the droplet has an initial tangential velocity (V_t), with respect to the wall, in the x direction. In oblique impact, normal Weber number (Wen), which is the Weber number based on droplet velocity normal to the wall, (V_n), is the dominant parameter. In this simulation, the initial normal and tangential velocities are equal to 0.52 m/s and 0.2 m/s, respectively. The corresponding normal Weber number is 10. Figure 5 represents the motion and deformation of the droplet during the impact process. The general behavior of the droplet is similar to the normal impact process. First, the droplet spreads over the surface and reaches its maximum spreading extent. In this case, a dimple is formed in the centre of the droplet. Then, the droplet retracts and reduces its spreading area. Finally, the droplet, due to its kinetic energy, rebounds from the surface. Contrary to normal impact, in this case, the droplet is displaced in the x direction and loses its symmetry as a result of its initial tangential velocity.

Figure 6(a) shows the temperature distribution around the droplet at t = 6.2 ms in the plane perpendicular to the z axis at the origin. As previously mentioned, the temperature inside the droplet is constant. A high temperature gradient can be observed in the vapor layer. The vapor layer between the droplet and the surface is also noticeable in this figure. Due to the high temperature gradient near the droplet bottom, the vaporization rate is higher in this region. Figure 6(b) represents the corresponding vaporization rate distribution in a band around the interface. As observed, using the proposed procedure, a smooth distribution of vaporization rate is obtained around the interface.

The residence time of the droplet on the surface, in this case, is 0.013 s. When the Weber number increases to 30, this time becomes about 0.012 s. It is concluded from our simulations that the residence time of the droplet in the regular reflection regime has a weak dependence on the impact velocity. This was also previously reported by Biance et al. [5] for a normal impact process.

4.2.1. Maximum spreading radius

In this section, the effect of normal Weber number on the maximum spreading radius, R_m, is considered. Biance et al. [5] experiments showed that the spreading factor (R_m/R) is proportional to the fourth root of the Weber number for the normal impact case. Figure 7 shows the variations of the spreading factor with the normal Weber number. Other parameters are the same as previous simulations. The best analytical fit to the numerical results is coincident with the following

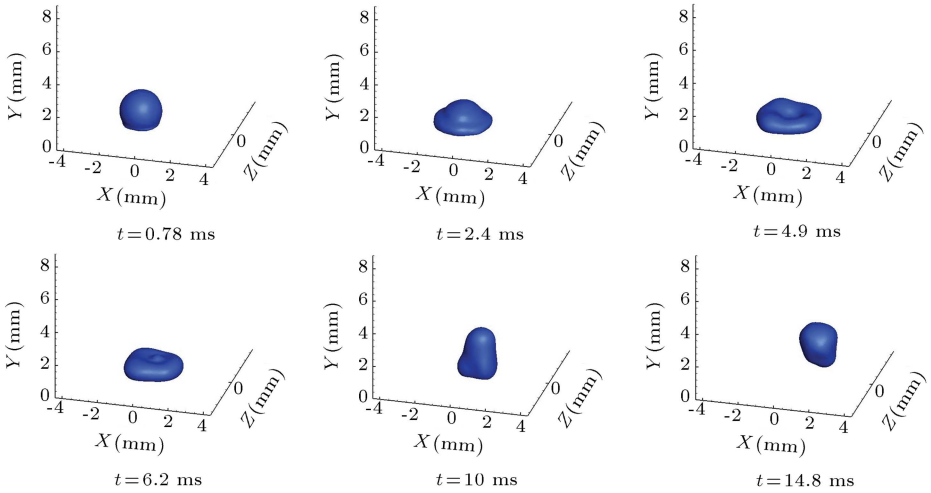

Figure 5. Droplet deformation during an oblique impact process (Wen = 10, Vt = 0.2 m/s, D = 2.3 mm and T_w = 400°C).

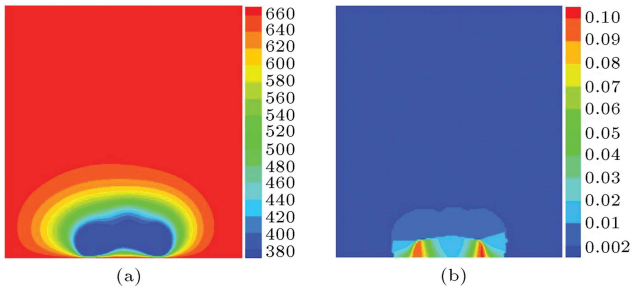

Figure 6. Temperature (a) and vaporization rate (b) contours at t = 6.2 ms for the impact of Figure 5.

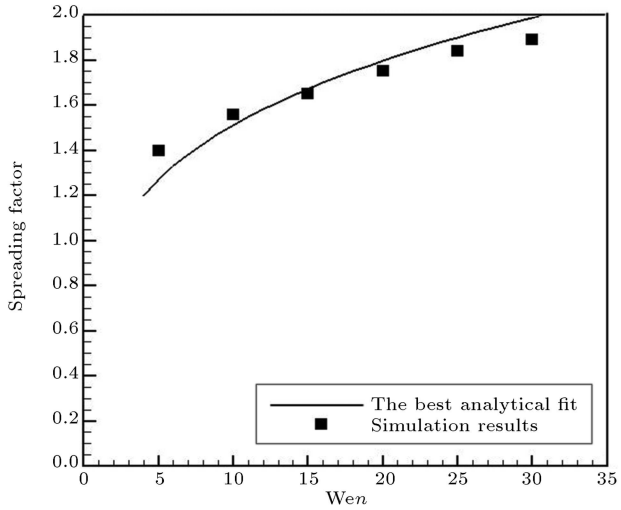

Figure 7. Spreading factor (R_m/R) as a function of the normal Weber number.

equation:

$$\frac{R_m}{R} = 0.85\,\mathrm{We}n^{1.4}. \tag{29}$$

Therefore, in the oblique impact process, the spreading factor is proportional to the fourth root of the normal Weber number.

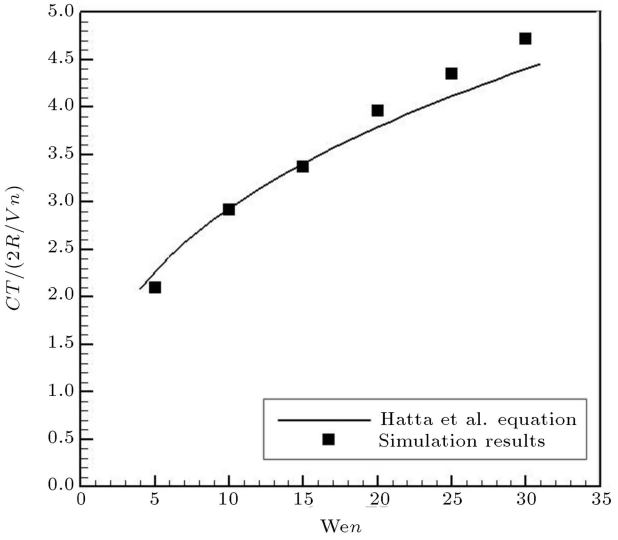

Figure 8. Non-dimensional contact time as a function of the normal Weber number.

4.2.2. Contact time

Hatta et al. [2] presented an empirical relation for estimation of the contact time of a droplet on a surface in the film boiling regime as:

$$CT/(2R/Vn) = 1.25\,\mathrm{We}n^{037}. \tag{30}$$

In the above equation, CT and Vn represent contact time and the initial normal velocity of the droplet, respectively.

The variations of the contact time with the normal Weber number can be seen in Figure 8. As observed, our numerical results are in good agreement with experimental results (Eq. (30)).

4.2.3. Heat transfer analysis

In this section, the effect of impact angle and also Weber number on heat transfer is considered. In order to examine the effect of Weber number on the

heat transfer rate from the wall, consider three normal impacts with initial normal velocities of 0.52 m/s, 0.73 m/s and 0.89 m/s, corresponding to normal Weber numbers of 10, 20 and 30, respectively. Figures 9 and 10 represent the time variations of the heat transfer rate and total heat removal from the surface for these three impact processes. In these figures, we made the time dimensionless using the contact time calculated by Eq. (30). An increase in the normal Weber number leads to the reduction of the vapor layer average thickness in the spreading stage. This results in enhancement of the vertical temperature gradient on the surface. On the other hand, the heat transfer area is higher for impacts with higher normal Weber number. Therefore, heat transfer rate and, consequently, total heat removal from the surface is increased with an increase in the normal Weber number. In Figure 9, the maximum heat transfer rate is related to the end of the spreading stage, where the contact area reaches its maximum value. Note that due to the equality of initial gas temperature and surface temperature, the computed heat loss is mainly related to the droplet impact.

Now, simulations are carried out for a constant Weber number (We = 10) and different impact angles. Figures 11 and 12 show the variations of the heat

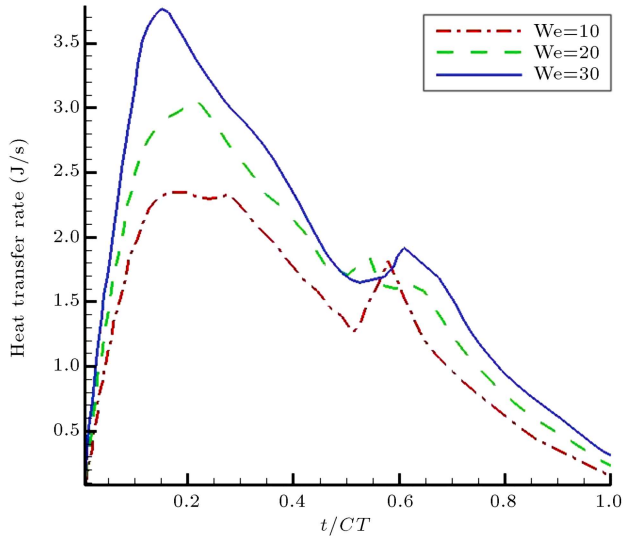

Figure 9. The effect of the Weber number on the heat transfer rate from the surface ($D = 2.3$ mm and $T_w = 400°C$).

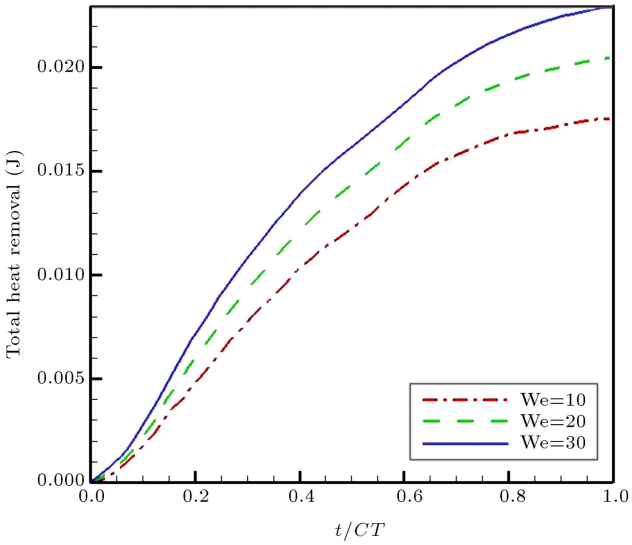

Figure 10. The effect of the Weber number on the heat removal rate from the surface ($D = 2.3$ mm and $T_w = 400°C$).

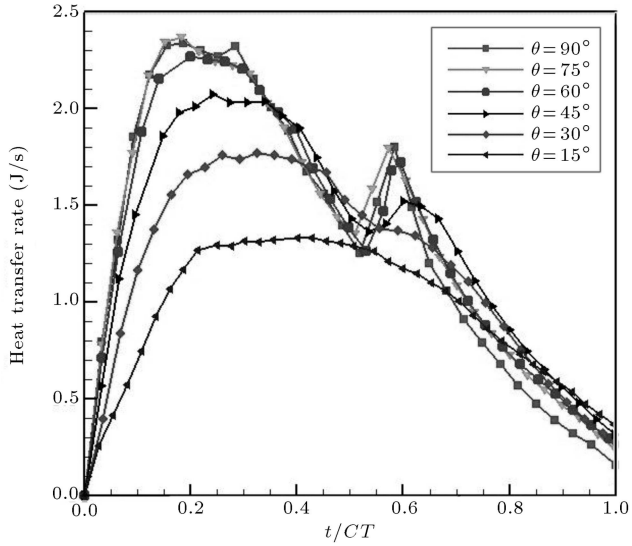

Figure 11. The effect of the impact angle on the heat transfer rate from the surface (We = 10, $D = 2.3$ mm and $T_w = 400°C$).

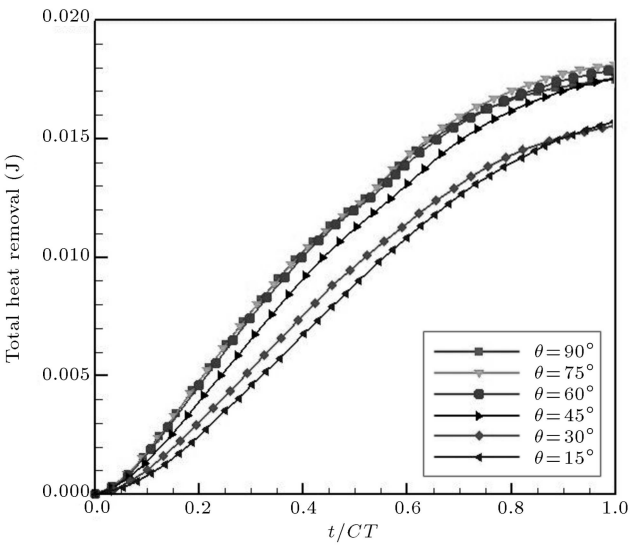

Figure 12. The effect of the impact angle on the heat transfer rate from the surface (We = 10, $D = 2.3$ mm and $T_w = 400°C$.

transfer rate and total heat removal from the wall for different impingement angles, respectively. A reduction in the impact angle results in a reduction of the normal impact velocity. Therefore, the averaged vapor layer thickness in the spreading stage increases. This leads to a reduction in the normal temperature gradient. In addition, reduction of the normal impact velocity is accompanied with the reduction of the heat transfer area in the spreading stage. As a result, for lower impact angles of 15° and 30°, heat transfer rate and, consequently, total heat removal decreases noticeably. The heat transfer rate for impact angles of 15° and 30° is very different. But, the total heat removal for these two cases is almost the same at the end of the impact process. This is due to the difference of the droplet contact time for these cases. For all impact angles, except 15°, impact occurs in the large deformation regime ($We_n > 1$), and the droplet contact time is almost constant (about 12 ms). For an impact angle of 15°, the droplet impact occurs in the quasi elastic regime ($We_n < 1$). In this regime, the droplet contact time is longer (about 16 ms). Therefore, the total heat removal increases for this case.

5. Conclusions

This paper focuses on a more accurate simulation of the oblique impact of a droplet on a wall in the film boiling regime. The level set method was applied to track the interface. Also, the ghost fluid method was employed to handle discontinuities at the interface. In order to have sufficient mesh resolution in the vapor layer, mesh was clustered near the wall. Since accurate computation of the vaporization rate has a significant effect on our numerical method, a robust procedure was proposed for accurate calculation of the vaporization rate.

First, the normal impact of a water droplet on a superheated wall was simulated, and the agreement between simulation results and experiments was satisfactory. Then, the oblique impact process of a water droplet on a superheated wall in the regular reflection regime was simulated, and the results were verified against experiments.

According to our simulations, the normal Weber number (Weber number based on the normal velocity of the droplet) has a dominant effect on the regular reflection regime. The spreading factor in this regime is proportional to the fourth root of the normal Weber number. Also, the non dimensional contact time of the droplet on the surface is a function of normal Weber number. Droplet contact time has a weak dependence on the normal impingement velocity.

The effect of Weber number and impact angle on total heat removal from the wall was considered. In the normal impact process, an increase in the normal Weber number of the droplet increases the heat transfer rate and, consequently, the total heat removal from the surface. When the droplet impacts on a surface with an angle lower than 45°, a noticeable reduction in total heat removal occurs. Therefore, impact angles greater than 45° and, especially, normal impact, are suggested for a more efficient cooling process.

Nomenclature

x	x direction
y	y direction
z	z direction
τ	Time (s)
$\vec{V}$	Velocity vector (ms^{-1})
u	Velocity component in x direction (ms^{-1})
v	Velocity component in y direction (ms^{-1})
w	Velocity component in z direction (ms^{-1})
p	Pressure (Nm^2)
$\vec{g}$	Gravity vector (ms^{-2})
T	Temperature (K)
k	Thermal conductivity ($Wm^{-1}K^{-1}$)
C_p	Specific heat at constant pressure ($Jkg^{-1}K^{-1}$)
$\dot{m}$	Vaporization rate per unit surface ($kgm^{-2}s^{-1}$)
$\vec{N}$	Unit normal vector
$\vec{T}_1, \vec{T}_2$	Orthogonal unit tangent vectors
h_{lg}	Latent heat of vaporization (Jkg^{-1})
D	Droplet diameter (m)
R	Droplet radius (m)
V	Droplet initial velocity (ms^{-1})
Vn	Droplet initial normal velocity (ms^{-1})
Vt	Droplet initial tangential velocity (ms^{-1})
We	Weber number
We_n	Normal Weber number (based on the droplet normal velocity)
CT	Droplet contact time (s)
R_m	Maximum spreading radius of droplet (m)
CPR	Cell per droplet radius
V_d	Droplet volume (m^3)
ρ	Density (kgm^{-3})
μ	Viscosity ($Nm^{-2}s$)

∇	Gradient operator
σ	Surface tension (Nm^{-1})
κ	Curvature (m^{-1})
φ	Level set function (m)
τ	Pseudo time (s)
Γ	Interface

Subscripts

x	Derivative in x direction
y	Derivative in y direction
z	Derivative in z direction
l	Liquid
g	Gas
w	Wall
int	Interface
sat	Saturation
n	Normal derivative

References

1. Wachters, L.H.J. and Westerling, N.A.J. "The heat transfer from a hot wall to impinging water drops in the spheroidal state", *Chem. Eng. Sci.*, **21**, pp. 1047-1056 (1966).
2. Hatta, N., Fujimoto, H., Kinoshita, K. and Takuda, H. "Experimental study of deformation mechanism of a water droplet impinging on hot metallic surfaces above the Leidenfrost temperature", *J. Fluids Eng.*, **119**, pp. 692-699 (1997).
3. Karl, A. and Frohn, A. "Experimental investigation of interaction process between droplets and hot walls", *Phys. Fluids*, **12**, pp. 785-796 (2000).
4. Kang, B.S. and Lee, D.H. "On the dynamic behavior of a liquid droplet impacting upon an inclined heated surface", *Exp. Fluids*, **29**, pp. 380-387 (2000).
5. Biance, A.L., Chevy, F., Clanet, C., Lagubeau, G. and Quere, D. "On the elasticity of an inertial liquid shock", *J. Fluid Mech.*, **554**, pp. 47-66 (2006).
6. Chen, R.H., Chiu, S.L. and Lin, T.H. "On the collision behaviors of a diesel drop impinging on a hot surface", *Exp. Therm. Fluid Sci.*, **32**, pp. 587-595 (2007).
7. Karl, A., Anders, K., Rieber, M. and Frohn, A. "Deformation of liquid droplets during collisions with hot walls: Experimental and numerical results", *Part. Part. Syst. Charact.*, **13**, pp. 186-191 (1996).
8. Harvie, D.J.E. and Fletcher, D.F. "A hydrodynamic and thermodynamic simulation of droplet impacts on hot surfaces, Part I: Theoretical model", *Int. J. Heat Mass Transfer*, **44**, pp. 2633-2642 (2001).
9. Harvie, D.J.E. and Fletcher, D.F. "A hydrodynamic and thermodynamic simulation of droplet impacts on hot surfaces, Part II: Validation and applications", *Int. J. Heat Mass Transfer*, **44**, pp. 2643-2659 (2001).
10. Ge, Y. and Fan, L.S. "Three-dimensional simulation of impingement of a liquid droplet on a flat surface in the Leidenfrost regime", *Phys. Fluids*, **17**, pp. 1-20 (2005).
11. Chatzikyriakou, D., Walker, S.P., Narayanan, C. and Lakehal, D. "Comparison of measured and modeled droplet-hot wall interactions", *Appl. Therm. Eng.*, **29**, pp. 1398-1405 (2009).
12. Fedkiw, R.P., Aslam, T., Merriman, B. and Osher, S. "A non-oscillatory Eulerian approach to interfaces in multimaterial flows (the ghost fluid method)", *J. Comput. Phys.*, **152**, pp. 457-510 (1999).
13. Liu, X.D., Fedkiw, R.P. and Kang, M. "A boundary condition capturing method for Poisson's equation on irregular domains", *J. Comput. Phys.*, **160**, pp. 151-178 (2000).
14. Nguyen, D.Q., Fedkiw, R.P. and Kang, M. "A boundary condition capturing method for incompressible flame discontinuities", *J. Comput. Phys.*, **172**, pp. 71-98 (2001).
15. Gibou, F., Chen, L., Nguyen, D. and Banerjee, S. "A level set based sharp interface method for the multiphase incompressible Navier-Stokes equations with phase change", *J. Comput. Phys.*, **222**, pp. 536-555 (2007).
16. Kang, M., Fedkiw, R.P. and Liu, X.D. "A boundary condition capturing method for multiphase incompressible flow", *J. Sci. Comput.*, **15**, pp. 323-367 (2000).
17. Tanguy, S., Menard, T. and Berlemont, A. "A level set method for vaporizing two-phase flows", *J. Comput. Phys.*, **221**, pp. 837-853 (2007).
18. Osher, S. and Fedkiw, R., *Level Set Methods and Dynamic Implicit Surfaces*, Springer-Verlag, New York, USA (2002).
19. Mehravaran, M. and Kazemzadeh Hannani, S. "Simulation of buoyant bubble motion in viscous flows employing lattice Boltzmann and level set methods", Sci. Iran., **18**, pp. 231-240 (2011).
20. Sussman, M., Smereka, P. and Osher, S. "A level set approach for computing solutions to incompressible two-phase flow", *J. Comput. Phys.*, **114**, pp. 146-159 (1994).
21. Son, G. and Dhir, V.K. "Numerical simulation of nucleate boiling on a horizontal surface at high heat fluxes", *Int. J. Heat Mass Transfer*, **51**, pp. 2566-2582 (2008).
22. Aslam, T.D. "A partial differential equation approach to multidimensional extrapolation", *J. Comput. Phys.*, **193**, pp. 349-355 (2003).

Biographies

Pedram Pournaderi received his BS degree in Mechanical Engineering (Heat and Fluids) from Semnan University, Iran, in 2002, and MS and PhD degrees in

Mechanical Engineering (Energy Conversion) from Isfahan University of Technology, Iran, in 2004 and 2012, respectively. He is currently Assistant Professor of Mechanical Engineering at Yasouj University, Iran. His research interests include fluid dynamics, heat transfer, two phase flow and computational fluid dynamics.

Ahmad Reza Pishevar is Professor of Mechanical Engineering at Isfahan University of Technology, Iran, and is Editor-in-Chief of the Journal of Computational Methods in Engineering. His research interests include compressible unsteady flow, multi phase flows and CFD simulations.